Structure and Morphology of Hydroxylated Amorphous Alumina Surfaces

S. P. Adiga,*,† P. Zapol,*,†,‡ and L. A. Curtiss†,‡

Materials Science Division and Chemistry Division, 9700 South Cass Avenue, Argonne National Laboratory, Argonne, Illinois 60439

Received: January 5, 2007; In Final Form: March 8, 2007

The effect of hydroxylation on the surface structure of amorphous alumina is investigated using classical molecular dynamics simulations. It is found that the hydroxylated amorphous alumina surface is terminated by hydroxyl groups singly and doubly coordinated to aluminum. Root-mean-square roughness calculations and density profiles across the film indicate that hydroxylated surfaces are rougher than non-hydroxylated surfaces. The power spectrum identifies different vibrational stretching frequencies for the singly and doubly coordinated surface OH groups. The role of the surface OH groups in surface reactivity is discussed.

1. Introduction

Alumina has been extensively used in many technological applications including catalysis[1] and the microelectronics[2] industry. The physical and chemical properties of alumina surfaces play a central role in most of these applications. While there are a number of crystalline polymorphs of alumina, amorphous alumina is an important form as well. The amorphous form of alumina is present in the surface layer of air exposed aluminum as well as in alumina films grown electrochemically or by the atomic layer deposition (ALD) technique. Recently, anodic aluminum oxide (AAO) membranes with ordered nanopores have drawn much attention for their potential applications in catalysis and as templates for growing nanostructures.[3,4] One of the attractions of AAO is that the pores can be made to be highly aligned and ordered and, furthermore, that they can be uniformly modified to have a desired pore size down to 10 nm using the ALD technique.[3] An ALD coating provides not only a means to tune the pore size but also the ability to obtain uniform pore surfaces of a given composition. The applications of AAO membranes often depend on the surface reactivity and morphology, so it is of much interest to gain a detailed understanding of the structure of amorphous alumina surfaces.

Alumina surfaces are often hydroxylated with a surface concentration in the range of 3−15 nm^{-2}.[1] The concentration and type of hydroxyl groups play an important role in the reactivity of the surface. For example, surface hydroxyl groups are primary reaction sites during ALD growth of alumina,[5] and this is utilized in coating the pores of AAO membranes. FT-IR and Raman spectroscopies have recently revealed that coating AAO membranes with ALD alumina modifies the type of hydroxyl groups on the surface in addition to imparting a uniform surface composition.[3] The knowledge of the structure of hydroxylated amorphous alumina is thus crucial to better understand and control its surface properties relevant to many applications.

In a previous study, we have investigated the structure of non-hydroxylated amorphous alumina surfaces using atomistic molecular dynamics (MD) simulations.[6] These calculations showed that the amorphous alumina surface is oxygen terminated and that undercoordinated oxygen and aluminum atoms dominate the surface region. In this paper, the structure of amorphous alumina in the presence of hydroxyl groups is investigated using MD simulations. First, hydroxyl groups are introduced in a bulk amorphous alumina system by replacing randomly selected aluminum atoms with hydrogen atoms followed by the removal of an equal number of oxygen atoms to maintain electrical neutrality. This is equivalent to replacing one Al_2O_3 unit with a dissociated water molecule. We call it hydroxylation rather than hydration to emphasize that H is present only as OH groups. The structure is equilibrated to make bulk amorphous alumina with randomly distributed OH groups. We then cleave the surfaces from the bulk system and anneal the structure at 1000 K to form hydroxylated amorphous alumina surfaces. We investigate the effect of the concentration of the hydroxyl groups on the physical and chemical properties of the amorphous alumina structure. In particular, we address the effect of the hydroxyl concentration on the surface morphology, concentration profile, and vibrational spectra. We also discuss the types of surface OH groups, their concentration, and dynamics.

2. Computational Methods

The basic simulation methodology is described in our previous study on amorphous alumina surfaces.[6] A description of the interatomic potentials used and a brief explanation of the amorphous surface models are presented here.

2.1. Interatomic Potentials. The interatomic potentials used for alumina are of the Buckingham type derived by Matsui.[7] These potentials have been used successfully for studying liquid[8] and amorphous alumina in bulk.[9] The pair interaction potential between atoms i and j as a function of interatomic distance r_{ij} is given by

$$V(r_{ij}) = \frac{q_i q_j}{r_{ij}} + D(B_i + B_j)\exp\left(\frac{A_i + A_j - r_{ij}}{B_i + B_j}\right) - \frac{C_i C_j}{r_{ij}^{\,6}} \quad (1)$$

where the terms represent Coulomb, repulsive, and van der Waals contributions, respectively. Here $D = 4.184$ kJ $Å^{-1}$ mol^{-1} is the standard force constant. Since the interatomic potential derived by Matsui includes parameters only for Al and O, the

* Corresponding authors. E-mail: (S.P.A.) spadiga@anl.gov and (P.Z.) zapol@anl.gov.
† Materials Science Division.
‡ Chemistry Division.

10.1021/jp0701035 CCC: $37.00
Published on Web 05/03/2007

TABLE 1: Potential Parameters Used

	q (e)	A (Å)	B (Å)	C (Å^3 kJ$^{1/2}$ mol$^{-1/2}$)
Al	1.4175	0.78520	0.03400	36.82
O	−0.9450	1.82150	0.13800	90.61
H	0.4725	−0.17607[a]	−0.02462[a]	1.86285[a]

[a] These parameters are used for the short-range part of O−H interaction. The H−H and H−Al pairs interact through the Coulomb potential alone.

TABLE 2: Atomic Compositions of Systems Used in Simulations

at. % H (system)	Al	O	H	density (g/cm^3)
0 (D)	8550	12825	0	3.236
2.15 (A)	8100	12375	450	3.037
6.02 (B)	7335	11610	1215	2.858
7.95 (C)	6975	11250	1575	2.745

parameters for H needed to be determined. The parameters for the O−H interaction were derived by fitting the energy versus the O−H distance curve for an $Al(OH)_3$ cluster to density functional theory results calculated using Gaussian 03[10] at the B3LYP/6-31G* level of theory. The fitting was performed under the constraint that the charge on H is 0.4725 e to preserve the charge neutrality of the water molecule. The resulting fit gives an adequate description of O−H interaction energies in the vicinity of the minimum, as well as in the interatomic distance range corresponding to the hydrogen bonds. The interactions between Al−H and H−H pairs are considered to be purely electrostatic. The partial charges q, the repulsive radii A, the softness parameters B, and the van der Waals parameters C for Al, O, and H atomic species are listed in Table 1.

2.2. Simulation Details. All simulations were carried out in a microcanonical ensemble. An MD time step of 1 fs and a short-range interaction cutoff of 12 Å were used. The long-range Coulomb interactions were calculated using the Ewald summation method. The simulations were performed using the DL_POLY_2.13 code.[11]

2.3. Amorphous Surface Preparation. Three hydroxylated amorphous alumina surface models with a 2.1 (system A), 6 (system B), and 8 (system C) at. % H content along with a non-hydroxylated amorphous alumina surface model (system D) were obtained as follows. First, bulk amorphous samples of a given H content were formed starting from the non-hydroxylated bulk system. The non-hydroxylated bulk amorphous alumina sample of a density of 3.236 g/cm^3 was obtained using the procedure detailed in ref 6. The bulk system contained a total of 2375 aluminum and oxygen atoms in the stoichiometric Al_2O_3 ratio in a cubic box of side $a = 29.18$ Å. In this non-hydroxylated system, a chosen number of Al atoms at random positions was replaced by H atoms to achieve the desired H content. For every Al atom replaced by an H atom, one O atom was removed to maintain the charge neutrality of the system. Subsequent to adding H atoms, the MD box was replicated 3 times in the x and y directions such that the new system consisted of 9 times the original number of atoms and had box lengths of $a = b = 87.54$ Å and $c = 29.18$ Å. The numbers of Al, O, and H atoms in systems A−D along with their densities are listed in Table 2.

Then, the bulk systems thus created were heated to 3000 K and equilibrated for 300 ps. This was followed by quenching the systems to 300 K through intermediate temperatures. Free surfaces were created by abruptly making the periodic box longer in the z direction by 50 Å after the amorphous bulk sample was obtained. This resulted in a periodically repeated slab of alumina of a thickness of 29.18 Å with two surfaces of a supercell area of 87.54 Å × 87.54 Å perpendicular to the z axis. Following the surface formation, the slab was annealed at 1000 K for 1.2 ns to relax the surface. The temperature was scaled every five steps during the first 200 ps of annealing following which the system temperature stabilized and oscillated around 1000 K. Finally, simulations were carried out at 300 K for 1.2 ns. The system reached equilibration within the first 300 ps, and the potential energy oscillated around an average value. The sampling was performed over the final 600 ps.

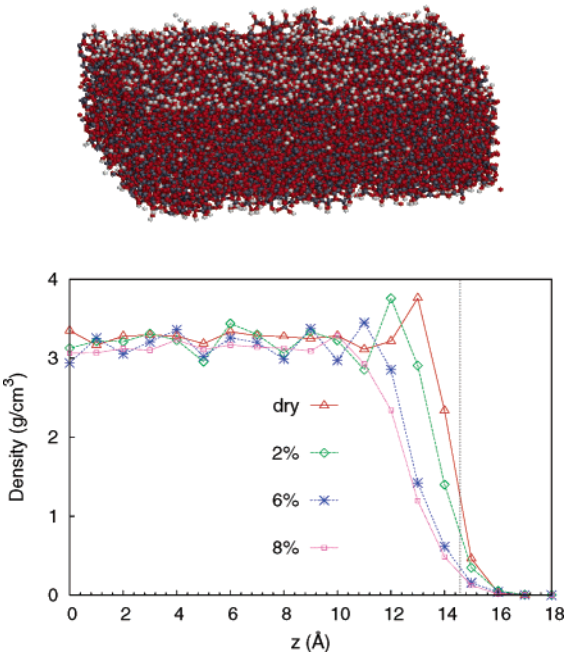

Figure 1. Top: ball-and-stick model of the hydroxylated amorphous alumina film. Al, O, and H are gray, red, and white, respectively. Note hydrogen termination of the surfaces. Bottom: density profile as a function of distance from the center of the film for 0, 2, 6, and 8% H containing systems. The values for layers of opposite z coordinates have been averaged. The dotted lines at $z = 14.59$ Å indicate original positions of the surface as cleaved.

3. Results and Discussion

A snapshot of system C depicted in the top panel of Figure 1 shows that the majority of the hydrogen atoms are near the surface. The density profiles as functions of the distance from the center of the slab for systems A−D are plotted in the bottom panel. The original cleaved bulk surfaces are 14.59 Å from the center of the slab. The surfaces relaxed from their original positions upon annealing as indicated by the first peak in the density profiles. The final density profiles extend to about 16 Å from the slab center for all systems considered. The density profiles are marked by peaks at 13, 12, 11, and 10 Å from the center of the slab for 0, 2, 6, and 8% H systems, respectively. After this first peak, the density profile assumes the bulk value a couple of angstroms into the surface. After surface relaxation, the bulk density values of 3.21, 3.17, 3.13, and 3.23 g/cm^3 are reached for systems A−D, respectively. This means that the extent of surface relaxation increased with the H content. As will be illustrated in the forthcoming section, the H atoms migrated to the surface region, making the surface OH terminated. It is evident that the first density peak and the density fluctuations become less prominent as the H content is increased.

3.1. Density Profiles and Coordination Number Profiles. The partial number density profiles of Al, H, and O are plotted in Figure 2 as a function of distance from the center of the slab ($z = 0$) for systems A (top), B (center), and C (bottom). The number density is calculated using layers of height $\Delta z = 1$ Å

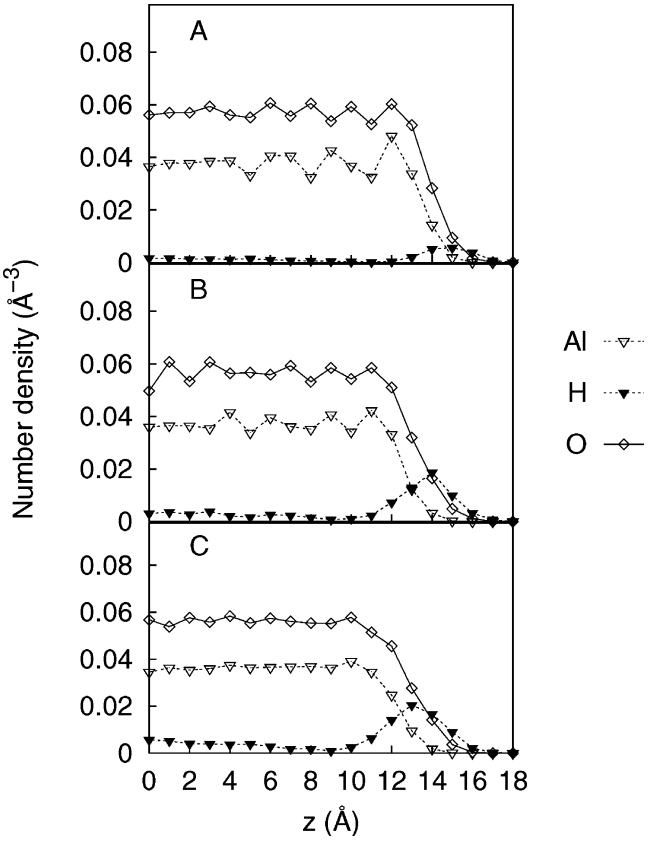

Figure 2. Number density profiles for Al, O, and H as functions of distance from the center of the film for systems with 2 (top), 6 (center), and 8 (bottom) atom % H. The values for layers of opposite *z* coordinates have been averaged.

parallel to the surfaces. It is clear from the density profiles that the H atoms have migrated from the interior of the film to the surface layers during the surface annealing. Thus, the surface OH concentration is much higher than the overall H content of the systems. If all the OH groups above the first maximum in the density (12, 11, and 10 Å for systems A−C, respectively) are considered to belong to the surface, the surface concentrations of hydroxyl groups are 1.82, 5.53, and 7.17 nm^{-2} for systems A−C, respectively. The H density profile reaches a maximum at $z = 15$, 14, and 13 Å for systems A−C, respectively. There are two differences in the density profiles of the hydroxylated surfaces as compared to the non-hydroxylated surface reported previously.[6] First, a hydroxylated surface is H terminated as compared to the non-hydroxylated surface, which is O terminated. Second, the subsurface layer Al peak and the oscillations in the density profile into the bulk become less prominent as the H content is increased. This is easy to explain based on Pauling's classic rules originally put forward for ionic crystals.[12] According to the first rule, the ions with a higher ratio of charge to ionic radius have higher coordination numbers. In hydroxylated alumina, the average coordination decreases from Al to O to H. The second rule states that in a stable anion (cation) coordination structure, the electric charge of each anion (cation) tends to compensate for the strength of the electrostatic valence bonds reaching to it from cations (anions) surrounding it. This means that lower coordinated atoms are preferred at the surface to minimize the number of broken bonds. Thus, lower coordinated H and O terminate hydroxylated and non-hydroxylated surfaces, respectively.

It is evident from decreases in both the magnitude of the first Al peak (Figure 2) and the density oscillations that the hydroxyl termination makes the surface less ordered. To analyze the effect

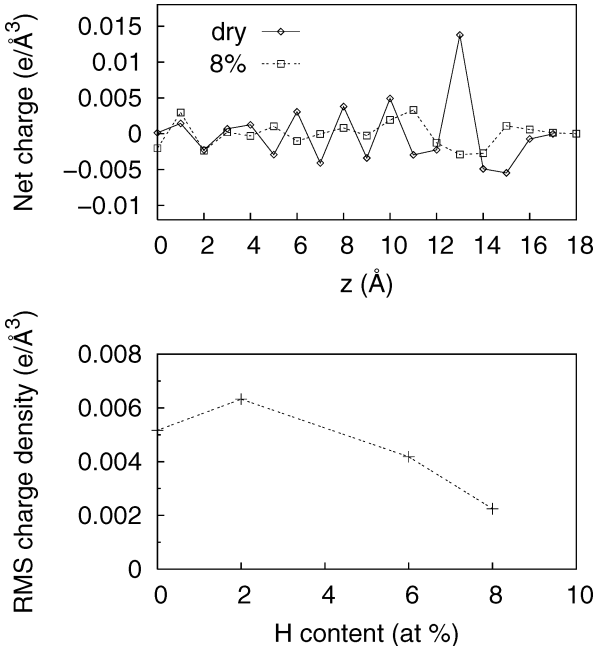

Figure 3. Top: net charge density profiles for dry and 8 atom % H systems. The values for layers of opposite *z* coordinates have been averaged. Bottom: rms charge density deviation across the film as a function of H content.

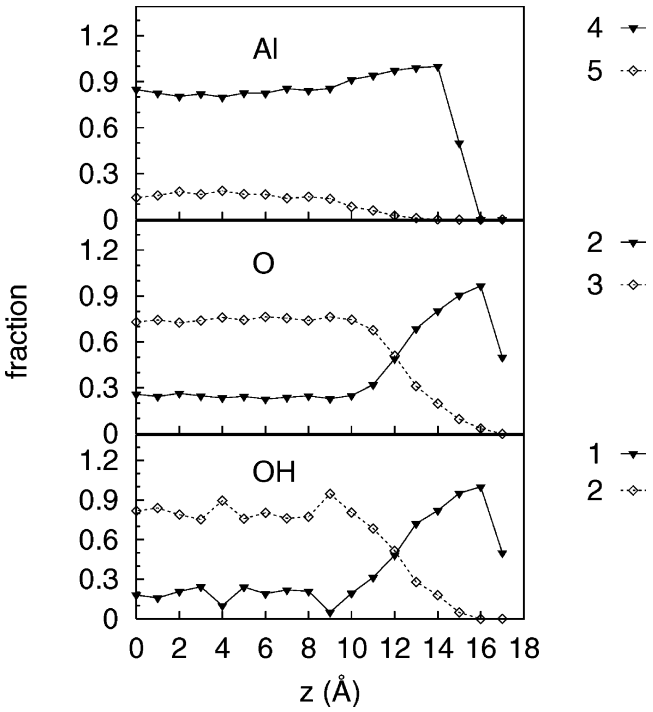

Figure 4. Number density profiles as functions of distance from the center of the film for 4- and 5-coordinated Al (top); 2- and 3-coordinated O (center); and 1- and 2-coordinated OH (bottom) for system C (8 atom % H). The values for layers of opposite *z* coordinates have been averaged.

quantitatively, the net charge density profiles across the film are shown for systems C (8 at. % H) and D (non-hydroxylated) in the top panel of Figure 3. The net charge density oscillations are more pronounced for the non-hydroxylated surface characterized by a strong peak near the surface corresponding to Al enrichment. The breaking of this preferential ordering by hydroxylation is quantified by calculating the root-mean-square (rms) of the net charge density deviation across the film. The rms charge density deviation is plotted as a function of H content

TABLE 3: Surface Concentration of OH Groups from MD Simulations[a]

	OH concentration (nm^{-2})		
system (at. % H)	OH(I)	OH(II)	total
A (2.15)	0.87	0.95	1.82
B (6.02)	3.59	1.94	5.53
C (7.95)	5.01	2.16	7.17

[a] A small concentration (<0.002 nm^{-2}) of OH groups coordinated to three Al atoms is not included in the table.

in Figure 3 (bottom panel). It is clear from the plot that hydroxylation brings down the layering in amorphous alumina surfaces.

Further insight into the effect of the surface on the short-range order can be obtained by analyzing the coordination numbers of the Al and O atoms. The coordination numbers are computed using cutoffs of 2.1 and 1.05 Å for the Al−O and the O−H bond distances, respectively. In Figure 4 (top panel), the fractions of $n = 4$- and 5-coordinated Al atoms are plotted as functions of the distance from the center of the slab. The surface Al atoms are predominantly tetrahedral. The fraction of 4-coordinated Al is 1.0 at the surface and eventually assumes the bulk value (0.77) at distances below 10 Å from the center. The profiles for 5-coordinated Al gradually increase, from zero at the surface to the bulk value at distances from the center below 10 Å. The key difference between the non-hydroxylated and the hydroxylated surfaces is the absence of 3-coordinated Al in the latter. This is mainly because the surface is H terminated and the Al atoms are pushed much further down below the surface. In the center panel of Figure 4, the fractions of $n = 2$- and 3-coordinated O atoms are plotted as functions of distance from the center of the slab. Oxygen atoms at the surface are predominantly 2-coordinated. It is noted that both O−H and O−Al bonds are included while determining the coordination number of O atoms. Going toward the center of the slab, the fraction of 2-coordinated oxygen atoms decreases parallel with an increase in 3-coordinated O, and these assume bulk values. Thus, in terms of coordination numbers, surface effects are present as deep as 5 Å below the outermost layer. It is also important to analyze the coordination number distribution for OH groups, determined by the number of Al atoms bonded to the O of the OH group. This distribution follows a trend similar to that of the O-coordination number profile (bottom panel, Figure 4). The surface OH groups are predominantly singly coordinated (i.e., the O atoms are 2-coordinated (H−O−Al), with the rest being doubly coordinated (H−O $<^{\mathrm{Al}}_{\mathrm{Al}}$)). However, as one moves toward the center of the slab, the fractions of singly (OH(I)) and doubly (OH(II)) coordinated OH assume bulk values. In Table 3, OH(I), OH(II), and total OH concentrations on the surface are listed. The surface concentration of OH groups was calculated by including OH groups that were above the first peak in density (Figure 1). It is clear from these values that an increase in the surface OH concentration increases the fraction of the OH(I) groups at the expense of the OH(II) groups.

3.2. O−H Partial Radial Distribution Function. The partial radial distribution functions (PRDFs) for O−H pairs for the top surface layer of 1 Å thickness and the whole slab for system C are compared in Figure 5. The PRDF $g(r)$ is defined as

$$g_{\alpha\beta}(r) = \frac{\langle n_{\alpha\beta}(r,\Delta r)\rangle}{4\pi r^2 \Delta r \rho_\beta} \qquad (2)$$

where $\langle n_{\alpha\beta}(r,\Delta r)\rangle$ is the average number of atoms of species β in a spherical shell of Δr at a distance r from an atom of species α, and ρ_β is the number density of atoms of species β. A value of $\Delta r = 0.02$ Å is used. The PRDF for the top 1 Å layer included atom pairs only if both atoms belonged to the layer. The first peak in the PRDF for the top layer is at 0.91 Å as compared to 0.93 Å for the whole slab. This is because at the surface, the OH groups are predominantly singly coordinated, whereas in the interior of the slab, the OH groups are both singly and doubly coordinated. Also, at the surface, the OH groups have shorter bond lengths than the groups of the same coordination in the interior region of the slab as the former have a smaller number of higher order neighbors. In comparison, the average O−H bond length in the bulk system (not shown in Figure 5) is 0.95 Å. The average O−H bond distance (0.93 Å) in the slab systems is shorter than the average O−H bond length (0.95 Å) in the bulk system as the majority of the OH groups in the latter are at the surface. The enlargement of the PRDF shown in the inset of Figure 5 indicates a small hump in the range of 1.3−2.3 Å that is more prominent for the whole slab than the top layer. This corresponds to hydrogen bonds.

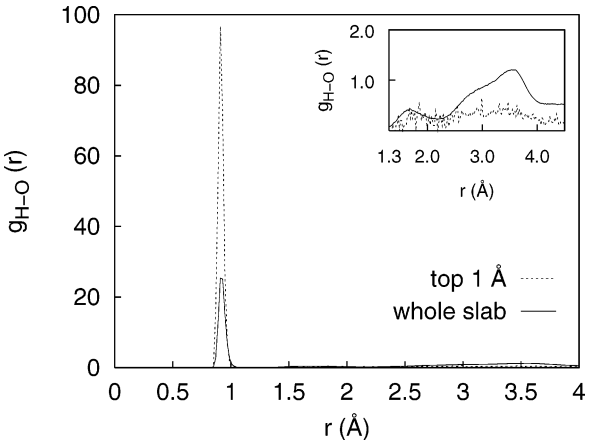

Figure 5. PRDF of O−H pair in the top 1 Å layer and in the interior of the surface of system C. The inset shows details of PRDF beyond the first peak starting at 1.3 Å.

Digne et al.[17] simulated several polymorphs of aluminum hydroxide with different degrees of hydration using first-principles density functional calculations with the Perdew−Burke−Ernzernhof functional. These polymorphs included gibbsite, bayerite, diaspore, boehmite, and tohdite. Oxygen in the OH groups of the hydroxides is 3-coordinated by one hydrogen and two aluminum atoms, with the notable exception of tohdite, where it is 4-coordinated. In comparison, our results show a predominance of 3-coordinated oxygen in the bulk of amorphous aluminum hydroxides. Their calculated O−H bond lengths fall between 0.93 and 1.028 Å, these values being somewhat higher than the X-ray diffraction results, which are not very accurate for hydrogen bond distances. The O−H bond length in our calculations is 0.95 and 0.91 Å in the bulk and at the surface, respectively. The bond length of hydrogen bonds in aluminum hydroxides was calculated to vary significantly, from 1.608 Å in diaspore to 2.36 Å in bayerite.[17] In comparison, the hydrogen bond length distribution in our simulations ranges from 1.3 to 2.3 Å with maxima at 1.65 and 1.9 Å in the bulk and at the surface, respectively.

3.3. Angle Distributions. In Figure 6, the Al−O−H angle distribution functions for 3 Å thick layers from the surface and from the interior of the film are compared for system C. A particular sequence of three atoms is included in the sampling for a layer if the center atom in the sequence belongs to that particular layer. To determine the bonded atoms, cutoff distances

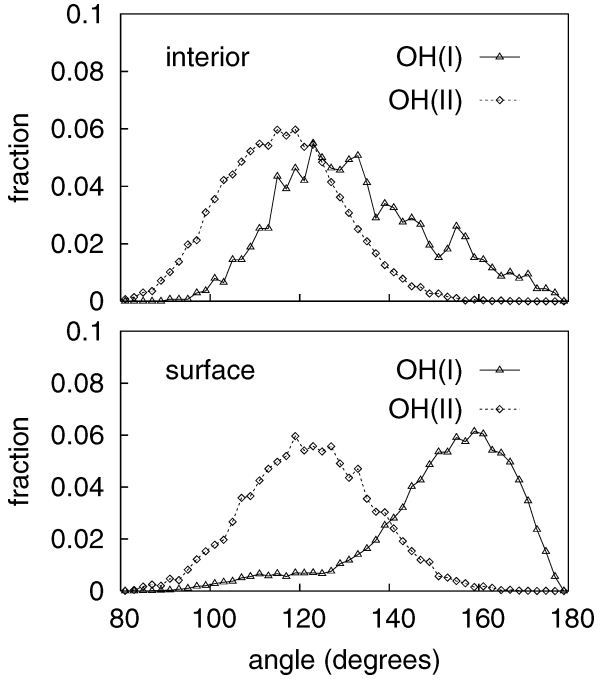

Figure 6. Al−O−H angle distributions for 3 Å interior (top) and surface (bottom) layers for system C. The distributions for OH(I) and OH(II) groups are plotted separately in each panel.

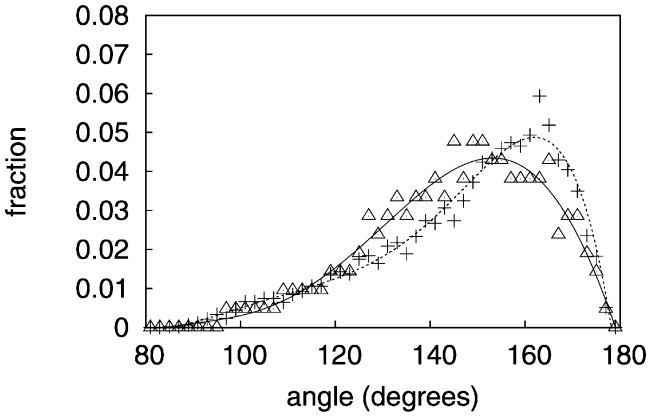

Figure 7. O−H−O angle distributions for 3 Å interior (triangles) and surface (crosses) layers for system C.

of 2.1 and 1.05 Å were used for the Al−O and O−H pairs, respectively. The aluminol angle distributions for the OH(I) and OH(II) groups are plotted separately. The Al−O−H angle distribution function for the interior OH(I) groups has a main peak at 123° and a small peak at around 155°. The distribution function for interior OH(II) groups has a peak around 118°. In comparison, the Al−O−H angle distribution functions for surface OH(I) and OH(II) have peaks around 160 and 122°, respectively. On the surface, the OH groups have less geometrical constraints allowing for Al−O−H angles close to 160°. In the interior, the OH(I) groups are constrained by the surrounding atoms, for example, by other O atoms in the bulk that form hydrogen bonds and restrict the Al−O−H angle to around 120°. It is important to point out that our model is limited by the use of a simple two-body interaction potential and that the angle distributions for aluminol groups presented are only meant for qualitative analysis.

The angle distribution for hydrogen bonded OH groups (O−H−O) in system C is plotted in Figure 7. An H−O pair is considered to be hydrogen bonded if the distance between the atoms is in the range of 1.3−2.3 Å corresponding to the hump following the first peak in the g_{O-H}. The O−H−O angle distribution has a wide range from 90 to 180° both in the bulk and at the surface. However, the maximum of the distribution at 155° in the bulk appears to be shifted to 150° for the surface. In comparison, the O−H−O (OH group hydrogen bonded to O) angle distribution in several crystalline aluminum hydroxides calculated using DFT[17] spans a broad range from 139.4° in bayerite to 178.8° in boehmite.

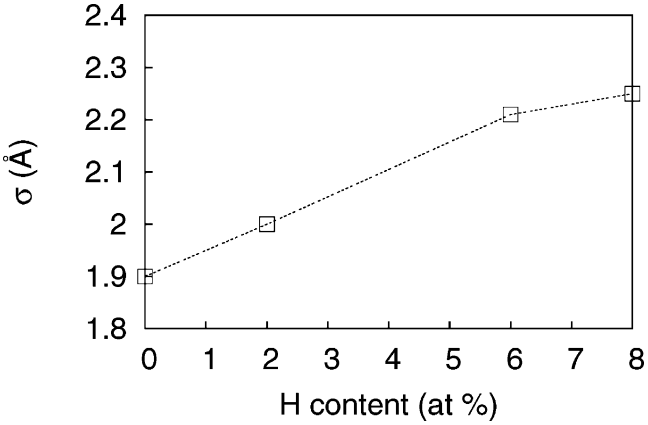

Figure 8. rms roughness as a function of H content.

3.4. Surface Roughness. To investigate the effect of hydrogen content on the roughness of the surfaces, the rms roughness of the surfaces was calculated as follows:

$$\sigma = \sqrt{<\langle z(x,y)^2\rangle - \langle z(x,y)\rangle^2>} \quad (3)$$

Here, z is the distance of the surface from the center of the slab as a function of the lateral position (x,y). The angle brackets indicate an average over square cells of 2 Å × 2 Å. The rms roughness is plotted as a function of at. % H in Figure 8. The effect of H is to increase the rms roughness of the surfaces from 1.9 to 2.3 Å. This is consistent with the diminishing first peak height with increasing H content that indicates a reduced surface order. Our data on the rms roughness can be compared to an experimental study of ALD Al_2O_3 films with a hydrogen content of about 5 at. %.[18] The rms roughness was measured using AFM in this study and was found to be 4 ± 1 Å, reasonably close to our value of 2.2 Å for the 6 at. % H system.

3.5. Vibrational Density of States. There have been a number of spectroscopic studies of hydroxylated alumina surfaces,[13,14] and the IR spectra of surface hydroxyl groups show a number of distinct bands, with several high-frequency peaks corresponding to vibrational OH stretch modes. The positions of these modes depend on the local atomic arrangement of the group. More recently, Xiong et al.[3] have studied the effect of ALD coating on the surface structure of AAO membranes. The FT-IR spectra of uncoated AAO membranes indicate the presence of two distinct types of OH stretches that were assigned to isolated OH and hydrogen bonded surface OH groups. Among the isolated surface OH groups, further distinction could be made depending on if the OH group is singly, doubly, or triply coordinated with Al. However, after ALD coating with alumina, the isolated peaks disappeared, and the spectra displayed a single broad band of hydrogen bonded surface OH groups, indicating a more dense coverage of OH groups. We have investigated the vibrational modes of the OH groups of the systems studied here and compared them with the experimental results.

The dynamics of surface OH groups is analyzed using vibrational power spectra (vibrational densities of states) calculated by following the atomic trajectories during the MD

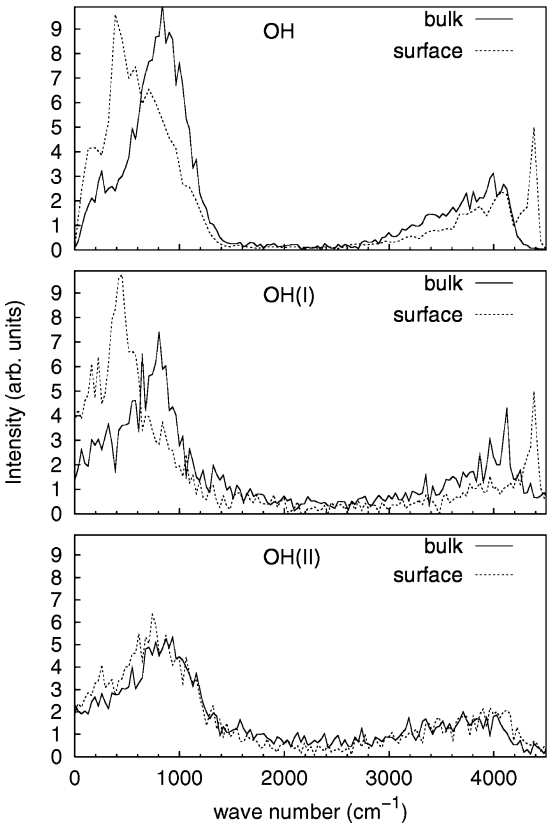

Figure 9. Vibrational density of states for all hydrogens (top) and hydrogens in singly (center) and doubly coordinated (bottom) OH groups in the bulk and surface systems.

simulation. We analyze the vibrational properties of the surface in terms of vibrational density of states (VDOS) of hydrogen atoms. The VDOS is determined by calculating the Fourier transform of the velocity auto-correlation function (VACF)

$$G(\omega) = \int \langle v(t)v(0)\rangle e^{i2\pi\omega t}\, dt \qquad (4)$$

The velocity autocorrelation function $\langle v(t)v(0)\rangle$ gives the correlation between the velocity of an atom at time $t = 0$ and the velocity of an atom at time $t = t$. The VDOS essentially contains the distribution of the power of atomic motions as a function of frequency sampled over an interval of simulation time. It is important to point out that the computed VDOS and the experimental IR or Raman vibrational spectra are not identical, as the former contains all vibrational atomic motions, and the latter have only IR or Raman active modes with intensities that are different than the computed VDOS. However, the calculated band positions and experimental spectra can be compared. Additionally, the simulations allow for computing the VDOS for individual atoms and separating out specific components of atomic/group motion, providing the basis for interpreting often complex experimental spectra. To calculate VACF, the velocities for H atoms were sampled every time step for 10 ps.

The overall VDOS of hydrogen atoms for both the bulk and the surface systems with 6 at. % H are shown in the top panel of Figure 9. The spectra for both systems are characterized by a set of intense bands below 1300 cm^{-1} and a set of relatively low-intensity bands in the high-frequency region above 3500 cm^{-1}. The major differences between bulk and surface densities lie in the high-frequency region above ~3500 cm^{-1} and in the low-frequency region below ~1300 cm^{-1}. The VDOS for the surface system have prominent peaks at ~4380, 4060, and 420 cm^{-1}. The two peaks in the high-frequency region correspond to vibrational OH stretching. The bulk system has peaks at 4000, 3860, and 780 cm^{-1}. By reference to density distribution of OH groups and their coordination number across the thickness (Figures 2 and 4) for the surface system, we anticipate that the VDOS are dominated by the OH(I) groups abundant near the surface layer. To further investigate the difference between the surface and the bulk system, VDOS for OH(I) (center panel) and OH(II) (bottom panel) groups are plotted separately in Figure 9. In the surface system, peaks that correspond to an OH stretch are at 4380 and 4000 cm^{-1} for the OH(I) and OH(II) groups, respectively. The corresponding spectra for the bulk system show peaks at 3980 and 3860 cm^{-1} for the OH(I) and OH(II) groups, respectively. Thus, the frequency of stretching vibrations is higher for singly coordinated OH than for doubly coordinated OH. This is consistent with experimental results, which place a stretch frequency of the terminal OH group coordinated by a single Al higher than that of a bridging OH group. The computed vibrational frequencies for OH(I) and OH(II) groups at the surface and in the bulk are listed in Table 4 along with experimental IR frequencies from ref 1. The computed frequencies for the OH stretches are much higher than the corresponding experimental values. This is not surprising given that the empirical fit did not include any vibrational properties. Also, even first-principles calculations tended to overestimate frequency values, which are often corrected by introducing a uniform scaling factor. For example, a factor of 0.9614 is typically used to correct frequencies calculated using the B3LYP exchange correlational functional within the DFT approach.[19] We have scaled the frequencies with a scaling factor obtained as follows. First, MD simulations at 300 K of bulk gibbsite are performed using the same interatomic potential. The VDOS for bulk gibbsite were computed, and the peak corresponding to the highest frequency in the OH stretching band was determined to be 4012 cm^{-1}. This value is compared against experimental values for the OH stretching frequencies. Gibbsite has a number of OH stretching frequencies detected by Raman spectroscopy in the range between 3363 and 3623 cm^{-1}.[20] The highest OH stretching frequency measured from IR spectroscopy is at 3617 cm^{-1}.[21] The ratio of these two values, 0.902, is used to scale the simulated OH stretch frequencies given in Table 3. The VDOS for the surface system are dominated by OH(I) groups predominant at the surface layer, whereas the VDOS for the bulk system are dominated by 2-coordinated OH groups. Further, since the surface OH groups have a lower average bond length, their stretching potential is much steeper than the OH groups in the bulk. Hence, in general, the stretching frequencies for surface OH groups are higher than the corresponding OH groups in the bulk.

TABLE 4: O−H Vibrational Frequencies (cm^{-1})

		present work		
system	OH group	non-scaled	scaled (scaling factor = 0.902)	exptl[3]
surface	OH(I)	4380	3950	3793
	OH(II)	4060	3662	3746
bulk	OH(I)	4000	3608	
	OH(II)	3860	3482	

Boehm and Knotzinger[22] noted that the OH stretch in aluminum hydroxides is red-shifted with an increase in bond length or with an increase in OH coordination. Thus, hydroxyls involved in hydrogen bonding or bridging hydrogens (OH(II)) exhibit bands at lower wavenumbers as compared to OH(I).

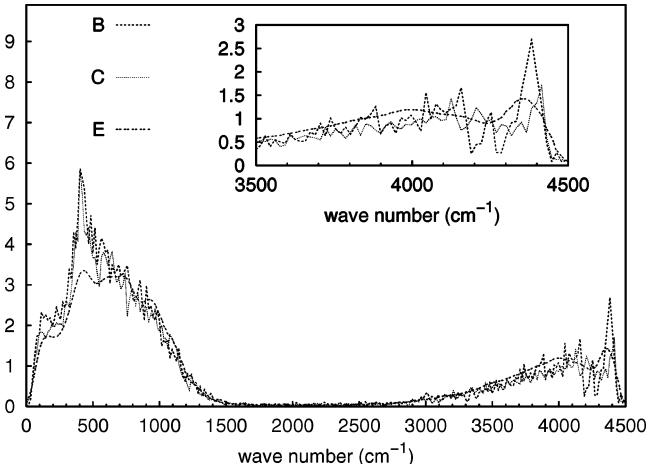

Figure 10. Vibrational density of states of H atoms for systems B, C, and E. The inset shows details of the high-frequency region.

Boehm and Knotzinger suggested that OH(I) is in the 3760−3800 cm^{-1} region and that OH(II) is in the 3740−3745 cm^{-1} region.

To analyze the effect of surface OH concentrations on the spectra, we have plotted the VDOS for systems B and C in Figure 10. For a more complete comparison, we have also calculated VDOS for a system with a higher surface OH concentration of 9.53 nm^{-2} (system E). This system was obtained by randomly placing OH and O (corresponding to dissociated water) species on both surfaces of system D. The system was annealed at 1000 K for 0.2 ns. The water molecules that formed were removed such that all H are in the form of OH groups attached to Al on the surface. The final system contained 8550, 14002, and 2354 Al, O, and H atoms, respectively. The VDOS for the three systems (Figure 10) show similar features. However, the peak corresponding to the OH(I) stretch for system E is not as prominent as that for systems B and C. This is despite the fact that system E has a higher concentration of OH(I) groups. This stems from the fact that a higher concentration of OH groups means a higher number of hydrogen bonds and an associated broadening of OH stretch bands. The broadening effect in system E is not as prominent as compared to observations in ALD coated alumina,[3] which has a much higher concentration of surface OH groups.

In the low-frequency region of the simulated spectra, the band of frequencies below 1000 cm^{-1} results from an overlap of different components of atomic motions involving Al−O−H groups. Previous experimental observations in crystalline aluminum hydroxides identified vibrational peaks in this region, for example, pseudo-boehmite shows main bands at 1080 and 860 cm^{-1}, which are, respectively, the hydroxyl bending and the Al−O stretching vibrations.[24] The decomposition of our computed spectra for hydrogen into individual components showed that the two prominent modes in the range of 300−1000 cm^{-1} are the Al−O−H bending and the out-of-plane motion of the Al and H atoms in an aluminol group. In the bulk, both motions are characterized by peaks at 800 cm^{-1} for OH(I) groups, while the OH(II) groups showed peaks at 900 and 870 cm^{-1} for bending and out-of-plane motions. In the surface systems, the peaks are red-shifted with a value of 770 cm^{-1} for both modes of OH(II) and the bending mode of OH(I), while the out-of-plane mode of the OH(I) groups is further red-shifted to 420 cm^{-1}. The lowering of the bending and out-of-plane frequencies at the surface is the result of the OH groups being exposed and experiencing less hindrance for motion. This explains the difference between the surface and the bulk spectra in the frequency range of 300−1000 cm^{-1}.

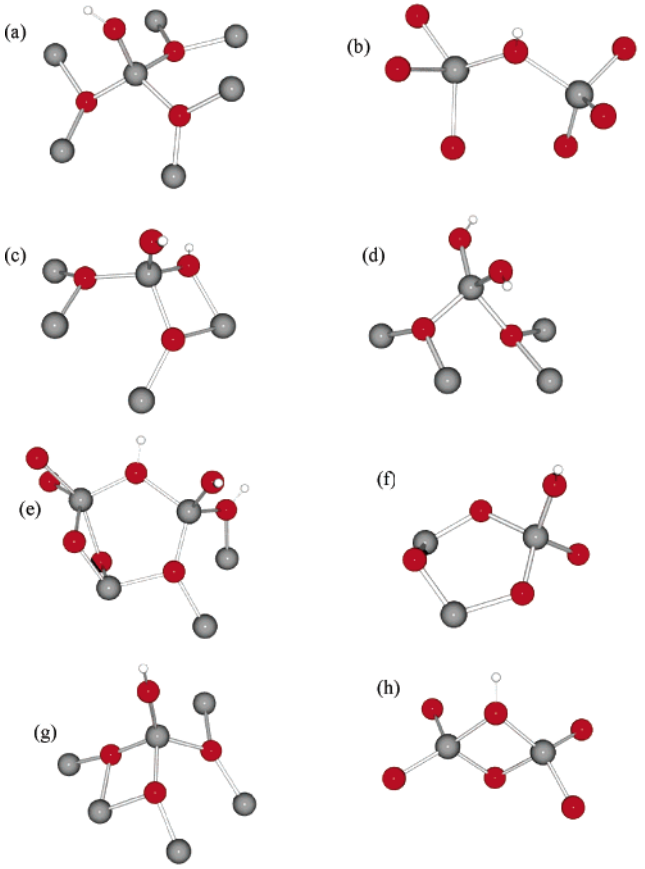

Figure 11. Representative surface OH groups. (a) OH(I)-AlO_3, (b) AlO_3-OH(II)-AlO_3, (c) OH(I)-Al-OH(II),O_2, (d) OH(I)-Al-OH(I),O_2, (e) OH(I)-Al-(OH(II))$_2$,O, (f) OH(I)-AlO_3 (3*n* ring), (g) OH(I)-AlO_3 (2*n* ring), and (h) AlO_3-OH(II) (2*n* ring) -AlO_3. Color code: Al (gray), O (red), and H (white).

3.6. Types of Surface OH Groups. It is possible to characterize surface OH groups based on the immediate chemical environment. There are predominantly two types of hydroxyl groups on the surface based on whether the OH is connected to one or two Al atoms (Figure 11a,b, respectively). There are also a few 3-coordinated OH groups (OH(III)) in the bulk; however, they are not statistically significant in either bulk or surface models studied here. In contrast, such groups are very prominent on α-alumina surfaces. It is well-known that the bridging OH(II) groups are more acidic than the singly coordinated OH(I) groups.[1] These two types of OH groups can be further classified considering the next nearest neighbors. As discussed previously, the majority of surface Al atoms are 4-coordinated. Hence, a surface OH(I) group has three second nearest neighbors. A 4-coordinated Al atom can be bonded to a maximum of three OH groups to remain a part of the amorphous network. These three second nearest neighbor positions can be filled with a combination of O, OH(I), or OH(II) species. Not distinguishing between 2- or 3-coordinated O, there is a total of six arrangements for OH(I) second nearest neighbors. In Figure 11, several different OH groups from the simulated system are depicted. An OH(I) (Figure 11a) or OH(II) (Figure 11b) group can be connected to an AlO_3 polyhedron. The OH(I) and OH(II) groups can be connected to Al atoms that are coordinated with more than one OH group. For example, the notation OH(I)−Al−OH(II),O_2 is used for an OH(I) group bonded to Al that is connected in addition to an OH(II) group and two O ions

coordinated only by aluminum atoms (Figure 11c). Similarly, OH(I)−Al−OH(I),O_2 is an OH(I) connected to Al atom bonded to another OH(I) group and two O ions (Figure 11d). The notation OH(I)−Al− $(OH(II))_2$,O is used for a OH(I) group bonded to an Al atom, which in turn is connected to one O and two OH(II) species (Figure 11e). As some combinations are statistically less probable, we have discussed only a few important species that are observed on the simulated surfaces. The OH groups can also be classified based on the ring size to which they are attached. For example, an OH(I) group can be connected to an Al atom that is a part of either a three membered (Figure 11f) or a two membered ring (Figure 11g). Similarly, an OH(II) group can be a part of a two (Figure 11h) or a three membered ring (not shown).

4. Conclusion

Amorphous alumina films with three different degrees of hydroxylation were studied using MD simulations. Surfaces were cleaved from bulk amorphous alumina samples with 2, 6, and 8 at. % H content. The majority of the hydrogen atoms migrated to the surface upon annealing at 1000 K, resulting in surface OH concentrations of 1.82, 5.53, and 7.17 nm^{-2}. The surface structure of the hydroxylated films was compared with dry amorphous alumina films. The hydroxylated amorphous alumina surfaces have two key differences as compared to dry surfaces. First, the surfaces are hydroxyl terminated as compared to O terminated non-hydroxylated alumina surface. Second, the subsurface Al enrichment in the O terminated, non-hydroxylated amorphous alumina surface disappears with increased loading by hydroxyl groups. Hydroxylation also alters the surface morphology marked by an increased surface roughness. The surface OH groups are either singly coordinated OH(I) or doubly coordinated OH(II) groups, with the latter type in the range from 30 to 50% of the total OH in the surfaces that we have studied. The fraction of OH(I) groups increases with surface OH concentration. The vibrational density of states of H atoms indicates the presence of distinct OH stretching modes corresponding to the OH(I) and OH(II) groups. The VDOS for the surfaces are dominated by the OH(I) stretching frequency as most of the OH groups are at the surface, and a majority of them are singly coordinated. The OH(II) groups are more reactive than OH(I) groups as they have a lower deprotonation energy. In contrast, ALD alumina has both a higher concentration of hydroxyl groups and a larger fraction of OH(I) groups. Thus, ALD alumina should be less catalytically active. The FT-IR spectra of ALD alumina are marked by a very broad band in the OH stretch region, which was explained by the presence of OH groups in very high concentrations.[3] The results of our simulations provide strong support for the suggestion of Xiong et al.[3] that in ALD alumina, which has a dense OH coverage, the vibrational peaks corresponding to isolated OH stretches disappear as a result of hydrogen bonding.

Acknowledgment. This work was supported by the US Department of Energy's Office of Basic Energy Sciences, under contract no. DE-AC02-06CH11357. Use of computer resources from Argonne National Laboratory Computer Resource Center and US DOE National Energy Research Supercomputer Center is gratefully acknowledged.

References and Notes

(1) Knozinger, H.; Ratnasamy, P. *Cat. Rev. Sci. Eng.* **1978**, *17*, 31.

(2) Gautier, M.; Fenaud, G.; Pham Van, L.; Villette, B.; Pollak, M.; Thromat, T.; Jollet, F.; Duraud, J. *J. Am. Ceram. Soc.* **1994**, *77*, 323.

(3) Xiong, G.; Elam, J. W.; Feng, H.; Han, C. Y.; Wang, H. H.; Iton, L. E.; Curtiss, L. A.; Pellin, M. J.; Kung, M.; Kung, H.; Stair, P. C. *J. Phys. Chem. B* **2005**, *109*, 14059.

(4) Pellin, M. J.; Stair, P. C.; Xiong, G.; Elam, J. W.; Birrell, J.; Curtiss, L. A.; George, S. M.; Han, C. Y.; Iton, L.; Kung, H.; Kung, M.; Wang, H.-H. *Cat. Lett.* **2005**, *102*, 127.

(5) Elliot, S. D. *Comp. Mat. Sci.* **2005**, *33*, 20.

(6) Adiga, S. P.; Zapol, P.; Curtiss, L. A. *Phys. Rev. B.* **2006**, *74*, 064204.

(7) Matsui, M. *Miner. Mag.* **1994**, *58A*, 571.

(8) Gutierrez, G.; Belonoshko, A. B.; Ahuja, R.; Johansson, B. *Phys. Rev. E* **2000**, *61*, 2723.

(9) Gutierrez, G.; Johansson, B. *Phys. Rev. B* **2002**, *65*, 104202.

(10) Gaussian 03, Revision C.02, Frisch, M. J.; Trucks, G. W.; Schlegel, H. B.; Scuseria, G. E.; Robb, M. A.; Cheeseman, J. R.; Montgomery, Jr., J. A.; Vreven, T.; Kudin, K. N.; Burant, J. C.; Millam, J. M.; Iyengar, S. S.; Tomasi, J.; Barone, V.; Mennucci, B.; Cossi, M.; Scalmani, G.; Rega, N.; Petersson, G. A.; Nakatsuji, H.; Hada, M.; Ehara, M.; Toyota, K.; Fukuda, R.; Hasegawa, J.; Ishida, M.; Nakajima, T.; Honda, Y.; Kitao, O.; Nakai, H.; Klene, M.; Li, X.; Knox, J. E.; Hratchian, H. P.; Cross, J. B.; Bakken, V.; Adamo, C.; Jaramillo, J.; Gomperts, R.; Stratmann, R. E.; Yazyev, O.; Austin, A. J.; Cammi, R.; Pomelli, C.; Ochterski, J. W.; Ayala, P. Y.; Morokuma, K.; Voth, G. A.; Salvador, P.; Dannenberg, J. J.; Zakrzewski, V. G.; Dapprich, S.; Daniels, A. D.; Strain, M. C.; Farkas, O.; Malick, D. K.; Rabuck, A. D.; Raghavachari, K.; Foresman, J. B.; Ortiz, J. V.; Cui, Q.; Baboul, A. G.; Clifford, S.; Cioslowski, J.; Stefanov, B. B.; Liu, G.; Liashenko, A.; Piskorz, P.; Komaromi, I.; Martin, R. L.; Fox, D. J.; Keith, T.; Al-Laham, M. A.; Peng, C. Y.; Nanayakkara, A.; Challacombe, M.; Gill, P. M. W.; Johnson, B.; Chen, W.; Wong, M. W.; Gonzalez, C.; and Pople, J. A.; Gaussian, Inc., Wallingford CT, 2004.

(11) DL_POLY is a molecular dynamics simulation package written by Smith, W.; Forester, T. R.; Todorov I. T. and has been obtained from CCLRC's Daresbury Laboratory via the website http://www.ccp5.ac.uk/DL_POLY.

(12) Pauling, L. J. *Am. Chem. Soc.* **1929**, *51*, 1010.

(13) Tsyganenko, A.; Filimonov, V. N. J. *Mol. Struct.* **1973**, *19*, 579.

(14) Tsyganenko, A. A.; Mardilovich, P. P. *J. Chem. Soc., Faraday Trans.* **1996**, *92*, 4843.

(15) Baumgarten, E.; Wagner, R.; Lentes-Wagner, C.; *Fresenius Z. Anal. Chem.* **1989**, *334* 246.

(16) Dyan, A.; Cenedese, P.; Dubot, P. *J. Phys. Chem. B* **2006**, *110* 10041.

(17) Digne, M.; Sautet, P.; Raybaud, P.; Toulhoat, H.; Artacho, E. *J. Phys. Chem. B* **2002**, *106*, 5155.

(18) Groner, M. D.; Fabreguette, F. H.; Elam, J. W.; George, S. M. *Chem. Mater.* **2004**, *16*, 639.

(19) Scott, A. P.; Radom, L. *J. Phys. Chem.* **1996**, *41*, 16502.

(20) Wang, S.-L.; Johnston, C. T. *Amer. Miner.* **2000**, *85*, 739.

(21) Gadsen, J. A. Infrared Spectra of Minerals and Related Inorganic Compounds, Butterworths, London, 1975.

(22) Boehm, H. P.; Knözinger, H.; *Nature and estimation of functional groups on solid surfaces.* In J. R. Anderson and M. Bouchart, Eds., Catalysis Science and Technology, **1983**, Springer, New York.

(23) Kubicki, J. D.; Apitz. S. E. *Amer. Miner.* **1998**, *83*, 1054.

(24) Kiss, A. B.; Kereztury, G.; Farkas, L. *Spectrochim. Acta, Part A* **1980**, *36*, 653.